# Articles

## Synthesis, Structure, and Flash Photolysis Kinetic Studies of Borylated Bis(dioximato)iron(II) Carbonyl Complexes

**D. G. A. Harshani de Silva, Daniel B. Leznoff, Gary Impey, Isak Vernik, Zhe Jin, and Dennis V. Stynes***

Department of Chemistry, York University, North York, Ontario, Canada M3J 1P3

*Received February 24, 1995*[⊗]

The synthesis and characterization of various borylated bis(dimethylglyoximato)iron complexes, $Fe(DMGBR_2)_2$-LL′ ($BR_2$ = $BH_2$, $BF_2$, $BPh_2$, or BBN (9-borabicyclo[3.3.1]nonane) and axial ligands L or L′ = pyridine, 1-methylimidazole, CO, butylamine, nitriles, $NH_3$, etc.) are described. Carbonyl complexes crystallize in the $C_{2v}$ conformation with both axial boron groups on the CO binding face. The bis(butylamine) complexes all show a $C_{2h}$ conformation. Flash photolysis studies of the carbonyl complexes and ligand substitution kinetics of other derivatives probe the linkage between the conformational dynamics of the macrocycle and the ligational dynamics of the iron complex. On-rate effects produced by groups which block access to the iron are compared with those for hemoproteins and superstructured hemes. Off-rate constants are largely unrelated to bond lengths or $\pi$-bonding/charge transfer effects. The off-rates reflect the true coordinate bond energy while structural and spectroscopic data only measure local phenomena. Electrochemical studies of $Fe(DMGBR_2)_2(PY)_2$ complexes and the nitrile complexes $Fe(DMGBPh_2)_2(PY)(RCN)$, RCN = 2,3-dichloro-5,6-dicyano-1,4-benzoquinone (DDQ) and tetracyanoethylene (TCNE), are described. Crystal data: $Fe(DMGBF_2)_2(PY)(CO)\cdot CH_2Cl_2$, orthorhombic space group $P2_12_12_1$, $a$ = 12.436(3) Å, $b$ = 13.246(2) Å, $c$ = 14.158(3) Å, $Z$ = 4; $Fe(DMGBPh_2)_2(PY)(CO)\cdot CH_2Cl_2$, orthorhombic space group $Pbcn$, $a$ = 14.943(3) Å, $b$ = 15.890(3) Å, $c$ = 16.211(3) Å, $Z$ = 4; $Fe(DMGBBN)_2$-(PY)(CO), monoclinic space group $P2_1/n$, $a$ = 11.611(2) Å, $b$ = 19.512(3) Å, $c$ = 14.907(2) Å, $\beta$ = 108.53(2)°, $Z$ = 4; $Fe(DMGBF_2)_2(BuNH_2)_2$, hexagonal space group $R\bar{3}$, $a$ = 27.874(4) Å, $c$ = 8.443(2) Å, $Z$ = 9; Fe-$(DMGBPh_2)_2(BuNH_2)_2$, monoclinic space group $P2_1/n$, $a$ = 13.928(3) Å, $b$ = 9.845(2) Å, $c$ = 15.288(3) Å, $\beta$ = 105.86(3)°, $Z$ = 2; $Fe(DMGBBN)_2(BuNH_2)_2$, monoclinic space group $Cc$, $a$ = 9.029(4) Å, $b$ = 19.303(9) Å, $c$ = 20.562(10) Å, $\beta$ = 92.790(1)°, $Z$ = 4.

### Introduction

A variety of increasingly sophisticated hemes[1-3] have been studied over the past decade. Prominent examples include chelated,[1a] picket fence,[1b] cyclophane,[2a] picnic basket,[2c] capped,[3a] jellyfish,[3b] basket handle,[3c] twin coronet,[3d] and face-to-face[3f] hemes. When superstructures are grafted onto the basic heme framework in order to introduce interactions with bound ligands, unintended structural distortions are often introduced which can lead to ambiguity or controversy in attempts to make quantitative arguments about superstructural effects.[2e,f]

Borylated dioxime complexes[4] of iron,[5,6] $Fe(DMGBR_2)_2$, provide a simple way of introducing axially pertinent superstructure while retaining some of the conformationally dynamic character of hemoprotein distal residues.[7] The $Fe(DMGBR_2)_2$ complexes can adopt either of the two conformations shown in Figure 1. The predominant solution conformers in the $BPh_2$ system were deduced on the basis of ring current shifted $^1H$ NMR resonances.[5a] The flipping of the phenyls from axial to equatorial sites is rapid on the NMR time scale and also rapid

[⊗] Abstract published in *Advance ACS Abstracts,* July 1, 1995.

(1) (a) Traylor, T. G. *Acc. Chem. Res.* **1981**, *14*, 102–109. (b) Collman, J. P. *Acc. Chem. Res.* **1977**, *10*, 265–272. (c) Suslick, K. S.; Reinert, T. J. *J. Chem. Educ.* **1985**, *62*, 974–979.

(2) (a) Traylor, T. G.; Tsuchiya, S.; Campbell, D.; Mitchell, M.; Stynes, D. V.; Koga, N. *J. Am. Chem. Soc.* **1985**, *107*, 604. (b) Collman, J. P.; Brauman, J. I.; Iverson, B. L.; Sessler, J. L.; Morris, R. M.; Gibson, Q. H. *J. Am. Chem. Soc.* **1983**, *105*, 3052–3065. (c) Collman, J. P.; Brauman, J. I.; Fitzgerald, J. P.; Hampton, P. D.; Naruta, Y.; Sparapany, J. W.; Ibers, J. A. *J. Am. Chem. Soc.* **1988**, *110*, 3477–3486. (d) Traylor, T. G.; Taube, D. J.; Jongeward, K. A.; Magde, D. *J. Am. Chem. Soc.* **1990**, *112*, 6875–6880. (e) David, S.; James, B. R.; Dolphin, D.; Traylor, T. G.; Lopez, M. A. *J. Am. Chem. Soc.* **1994**, *116*, 6–14. (f) Portela, C. F.; Magde, D.; Traylor, T. G. *Inorg. Chem.* **1993**, *32*, 1313–1320. (g) Ray, G. B.; Li, X.; Ibers, J. A.; Sessler, J. L.; Spiro, T. G. *J. Am. Chem. Soc.* **1994**, *116*, 162–176.

(3) (a) Hashimoto, T.; Dyer, R. L.; Crossley, M. J.; Baldwin, J. E.; Basolo, F. B. *J. Am. Chem. Soc.* **1982**, *104*, 2101–2109. (b) Uemori, Y.; Miyakawa, H.; Kyuno, E. *Inorg. Chem.* **1988**, *27*, 377–382. (c) Desbois, A.; Momenteau, M.; Lutz, M. *Inorg. Chem.* **1989**, *28*, 825–834. (d) Naruta, Y.; Tani, F.; Ishihara, N. Maruyama, K. *J. Am. Chem. Soc.* **1991**, *113*, 6865–6872. (e) Benson, D. R.; Valentekovich, R.; Diederich, F. *Angew. Chem., Int. Ed. Engl.* **1990**, *29*, 191–193. (f) Ward, B.; Wang, C. B.; Chang, C. K. *J. Am. Chem. Soc.* **1981**, *103*, 5236–5238.

(4) (a) Schrauzer, G. N. *Chem. Ber.* **1962**, *95*, 1438. (b) Bakac, A.; Brynildson, M. E.; Espenson, J. H. *Inorg. Chem.* **1986**, *25*, 4108–4114. (c) Shi, S.; Daniels, L. M.; Espenson, J. H. *Inorg. Chem.* **1991**, *30*, 3407–3410.

(5) (a) Stynes, D. V.; Leznoff, D.; de Silva, D. G. A. H. *Inorg. Chem.* **1993**, *32*, 3989–3990. (b) Impey, G. A.; Stynes, D. V. *J. Am. Chem. Soc.* **1993**, *115*, 7868–7869. (c) Stynes, D. V. *Inorg. Chem.* **1994**, *33*, 5022–5029. (d) Vernik, I.; Stynes, D. V. To be submitted for publication.

(6) (a) Thompson, D. W.; Stynes, D. V. *Inorg. Chem.* **1990**, *29*, 3815–3822. (b) Thompson, D. W.; Stynes, D. V. *Inorg. Chem.* **1991**, *30*, 636–640. (c) Thompson, D. W.; Noglik, H.; Stynes, D. V. *Inorg. Chem.* **1991**, *30*, 4567–4571. (d) Noglik, H.; Thompson, D. W.; Stynes, D. V. *Inorg. Chem.* **1991**, *30*, 4571–4575. (e) Vernik, I.; Stynes, D. V. Submitted for publication.

(7) (a) Case, D. A.; Karplus M. *J. Mol. Biol.* **1979**, *132*, 343–468. (b) Takano, T. *J. Mol. Biol.* **1977**, *110*, 569.

0020-1669/95/1334-4015$09.00/0 

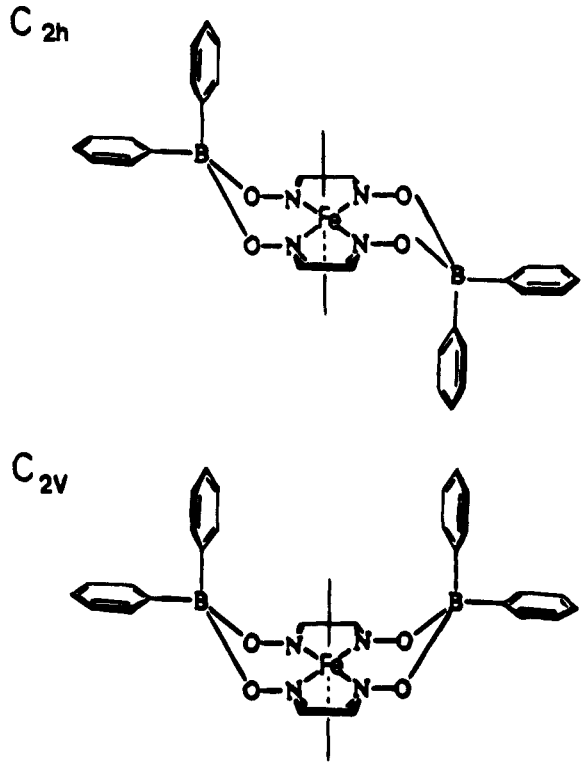


**Figure 1.** $C_{2h}$ and $C_{2v}$ conformations of $Fe(DMGBPh_2)_2$.

on the slower time scale of dissociative ligand substitution reactions. Axial boron-linked groups thus serve as flexible "gates" or conformationally mobile superstructure which may be positioned in close proximity to the axial binding sites of iron. These features have allowed us to observe effects of conformational flips on binding equilibria in $Fe(DMGBPh_2)_2$ complexes and to quantify the energetics of $\pi-\pi$ interactions between axial phenyls and bound ligands.[5b,c] Nonbonded effects range from strongly attractive 5 kcal/mol TCNE–phenyl interactions to 2–3 kcal/mol repulsive $\pi-\pi$ contacts with pyridine and aromatic nitriles. The borylated dioximes also produce low-spin Fe(III) complexes including novel ($\mu$-oxo)-diiron derivatives.[6d,e]

Less recognized, but also important, is the information which hemes and other $FeN_4$ systems provide concerning the fundamental nature of metal–ligand bonding.[8] A simple dissociative mechanism for ligand substitution[9] is well established, and one can often directly observe and study the pentacoordinate intermediate, as either a photochemical transient[1a] or a stable entity.[1a,b,6e] These features permit a detailed analysis of the reaction coordinate for ligand addition and dissociation.

In this work, we present synthetic, spectral, and electrochemical data for the new complexes, X-ray structural data for $BF_2$, $BPh_2$, and BBN complexes in both $C_{2v}$ and $C_{2h}$ conformations, and detailed kinetic studies of ligation to these systems. The results provide significant insights into important factors associated with the binding of ligands to metal complexes.

## Experimental Section

**Materials and Methods.** Diphenylborinic anhydride was freshly prepared from the commercially available diphenylboron ethanol amine ester.[10] The $Fe(DMGH)_2(PY)(CO)$, $Fe(DMGBF_2)_2(PY)_2$, and $Fe(DMGBF_2)(CH_3CN)_2$ complexes were prepared as described previously.[6a] Borane–dimethyl sulfide (2.0 M in THF) and 9-borabicyclo[3.3.1]nonane (0.5 M in THF) were purchased in sure-seal bottles and transferred via syringe. Dichloromethane was dried over $P_2O_5$ and distilled prior to use. Syntheses were carried out under a nitrogen atmosphere. Filtrations were carried out as rapidly as possible and wet solids dried immediately in vacuo.

**Physical Measurements.** Visible spectra were recorded on an Aminco DW2a or Cary 2400 spectrophotometer, infrared spectra as KBr disks on a Nicolet 20 SX-FTIR, and $^1H$ NMR spectra on a Bruker AM-300 instrument interfaced to an ASPEC 3000 computer. The flash photolysis system uses a conventional Applied Photophysics system interfaced via a digital storage oscilloscope to a microcomputer as described elsewhere.[6a] Elemental Analyses were obtained from Canadian Microanalytical Services, Delta, BC, Canada.

**Syntheses. (a) $Fe(DMGBPh_2)_2(PY)_2$.** Diphenylborinic anhydride (1.5 g, 4.33 mm) and $Fe(DMGH)_2(PY)(CO)$ (0.7 g, 1.78 mm) were allowed to react for 3 h under CO in warm $CH_2Cl_2$ (or until deemed fully borylated by visible spectroscopy). Pyridine (20 mL) and $CHCl_3$ (100 mL) were added, and the solution was warmed to 60 °C under a vigorous nitrogen purge (removing $CH_2Cl_2$), refluxed under nitrogen flow for 3 h, and then left to stand for 1 day. The volume was reduced and a red product precipitated on cooling and adding anhydrous ether. This was filtered off and dried in vacuo. Yield: 0.65 g. Anal. Calcd for $FeC_{42}H_{42}N_6O_4B_2$: C, 65.32; H, 5.48; N, 10.88. Found: C, 65.00; H, 5.34; N, 10.87. $^1H$ NMR ($\delta$, $CDCl_3$): 2.78 (dmg), 7.17, 6.83, 6.8 (Ph), 7.59, 6.36, 7.15 (PY). For the X-ray structure, see ref 5d.

**(b) $Fe(DMGBPh_2)_2(CH_3CN)_2$.** The $Fe(DMGBPh_2)_2(PY)_2$ product (0.35 g) was dissolved in $CH_2Cl_2$ (40 mL containing one drop of $CH_3CN$) under $N_2$, and the solution was diluted with 100 mL of $CH_3CN$. A yellow precipitate formed during removal of $CH_2Cl_2$ under a nitrogen purge and on standing overnight. The precipitate was filtered off and the above procedure repeated three times. The final yellow product was dried in vacuo. $^1H$ NMR ($\delta$, $CDCl_3$): 2.78 (dmg), 7.45, 7.11, 6.95 (Ph), 1.26 ($CH_3CN$). For the X-ray structure, see ref 5d.

**(c) $Fe(DMGBPh_2)_2(BuNH_2)_2$.** Butylamine (0.2 mL) was added to 2 mL of a dichloromethane solution of $Fe(DMGBPh_2)_2(PY)_2$ (50 mg), the mixture was stirred for 5 min, and hexane was added to induce precipitation of a red powder. The product was washed with hexane and dried in vacuo. Yield: 40 mg. $^1H$ NMR ($\delta$, $CDCl_3$): 2.81 (dmg), 7.37, 7.16, 7.07 (Ph), 0.65, 1.17, 0.26, 0.74, −0.64 ($BuNH_2$). For the X-ray structure, see Results.

**(d) $Fe(DMGBPh_2)_2(PY)(CO)$.** Carbon monoxide was bubbled through a solution of $Fe(DMGBPh_2)_2(PY)_2$ in $CH_2Cl_2$. The color of the solution rapidly changed from red to yellow. Hexane was added to precipitate the product. $^1H$ NMR ($\delta$, $CDCl_3$): 2.44 (dmg), 7.25, 7.0 ($Ph_{eq}$), 7.66, 7.25, 7.2 ($Ph_{ax}$), 9.02, 6.96, 7.65 (PY). IR ($cm^{-1}$): $\nu_{CO}$ = 2049, 2037. For the X-ray structure, see Results.

**(e) $Fe(DMGBPh_2)_2(PY)(TCNE)$.** To a $CH_2Cl_2$ (30 mL) solution of TCNE (17 mg, 0.13 mmol) was added $Fe(DMGBPh_2)_2(PY)_2$ (0.1 g, 0.13 mmol). After 5 min of stirring, the solvent was removed in vacuo. Yield: 0.11 g. Anal. Calcd for $FeC_{43}H_{37}N_9B_2O_4$: C, 62.88; H, 4.54; N, 15.35. Found: C, 62.13; H, 4.50; N, 15.31. $^1H$ NMR ($\delta$, $CDCl_3$): 2.60, 2.63 (dmg), 6.97, 7.68, 8.78 (PY), 7.0, 7.2, 7.28, 7.55 (Ph). IR ($cm^{-1}$): $\nu_{CN}$ 2178 (s), $\nu_{CC}$ 1452 (s). Vis ($\lambda_{max}$, nm (log $\epsilon$, $M^{-1}cm^{-1}$)): MOxCT , 430 (3.72); MAxCT, 1100 (3.90). For the X-ray structure, see ref 5d.

**(f) $Fe(DMGBPh_2)_2(CH_3CN)(TCNE)$.** The synthesis was similar to that above except that $Fe(DMGBPh_2)_2(CH_3CN)_2$ was used. $^1H$ NMR ($\delta$, $CDCl_3$): 2.75 (dmg), 2.03 ($CH_3CN$), 7.5, 7.23, 7.06, 6.93 (Ph). Vis ($\lambda_{max}$, nm (log $\epsilon$, $M^{-1}$ $cm^{-1}$)): MOxCT, 401 (3.74); MAxCT, 1055 (3.90).

**(g) $Fe(DMGBH_2)_2(PY)(CO)$.** To $Fe(DMGH)_2(PY)(CO)$ (1 g, 2.54 mmol) was added 2.7 mL of $BH_3$·$Me_2S$ (2.0 M in THF) dropwise. The complex dissolved with gas evolution. The solution was stirred

(8) Stynes, D. V. *Pure Appl. Chem.* **1988**, *60*, 561–566.
(9) (a) Chen, X.; Stynes, D. V. *Inorg. Chem.* **1986**, *25*, 1173–1182. (b) Stynes, D. V.; Fletcher, D.; Chen, X. *Inorg. Chem.* **1986**, *25*, 3483–3488. (c) White, D. K.; Cannon, J. B.; Traylor, T. G. *J. Am. Chem. Soc.* **1979**, *101*, 2443–2454. (d) Pang, I.; Stynes, D. V. *Inorg. Chem.* **1977**, *16*, 590–594.
(10) (a) Chremos, G. N.; Weidmann, H.; Zimmerman, H. K. *J. Org. Chem.* **1961**, *26*, 1683–1684. (b) Stephan, H.; Stephan, T. *Solubility of Inorganic and Organic Compounds*; Macmillan: New York, 1963; Vol. 1, Part 2, p 1053.

for 10 min, and then hexane was added to induce precipitation. The dark solid was filtered out, washed with $H_2O$ and then anhydrous ether, and dried in vacuo. Yield: 0.6 g, 57%. Anal. Calcd for $FeC_{14}H_{21}B_2N_5O_5 \cdot H_2O$: C, 38.67; H, 5.33; N, 16.11. Found: C, 38.79; H, 4.89; N, 15.94. $^1H$ NMR ($\delta$, $CDCl_3$): 2.23 (dmg), 8.85, 7.73, 7.29 (py). IR ($cm^{-1}$, KBr): $\nu_{BH}$ = 2426, 2352, $\nu_{CO}$ = 2022. Vis ($\lambda_{max}$, nm (log $\epsilon$, $M^{-1}$ $cm^{-1}$)): MOxCT, 404 (3.78).

**(h) Fe(DMGBH$_2$)$_2$(PY)$_2$.** A $CHCl_3$ (20 mL) solution of Fe(DMGBH$_2$)$_2$(PY)CO (300 mg) containing 1 mL of pyridine was refluxed under $N_2$ for 2 h. The $CHCl_3$ was stripped off in vacuo, and the product was precipitated by addition of methanol. The orange solid was filtered out, washed with hexane, and dried in vacuo. Yield: 0.17 g, 50%. $^1H$ NMR ($\delta$, $CDCl_3$): 2.56 (dmg), 6.96, 7.43, 8.02 (py). IR ($cm^{-1}$): $\nu_{BH}$ = 2394, 2367, 2310. Vis ($\lambda_{max}$, nm (log $\epsilon$, $M^{-1}$ $cm^{-1}$)): MOxCT, 518 (3.83); MPyCT, 384, 429.

**(i) Fe(DMGBH$_2$)$_2$(MeIm)$_2$.** The compound was prepared similarly to the pyridine complex above. $^1H$ NMR ($\delta$, $CDCl_3$): 2.51 (dmg), 3.47, 7.25, 6.94, 6.52 (MeIM). Vis ($\lambda_{max}$, nm (log $\epsilon$, $M^{-1}$ $cm^{-1}$)): MOxCT, 540 (4.84). IR ($cm^{-1}$): $\nu_{BH}$ = 2353, 2340.

**(j) Fe(DMGBBN)$_2$(PY)(CO).** A solution of BBN (8.5 mL of a 0.5 M solution in THF) was added to 0.8 g of Fe(DMGH)$_2$(PY)(CO) under a CO atmosphere in the dark. After 20 min, an additional 1.0 mL of the BBN reagent was added, and stirring was continued for 2 h until all $H_2$ evolution had ceased. Hexane was added (40 mL), and the yellow precipitate was filtered out, washed copiously with hexane, and dried in vacuo. Yield 1.1 g, 85%. (The product is slightly contaminated with colorless BBN side products.) Anal. Calcd for $FeC_{30}H_{45}N_5B_2O_5$: C, 56.91; H, 7.16; N, 11.56. Found: C, 54.62; H, 6.92; N, 11.06. $^1H$ NMR ($\delta$, $CDCl_3$): 2.23 (dmg), 8.80, 7.76, 7.28 (PY). IR ($cm^{-1}$): $\nu_{CH}$ = 2973, 2912, 2875, 2830, $\nu_{CO}$ = 2012. Vis ($\lambda_{max}$, nm (log $\epsilon$, $M^{-1}$ $cm^{-1}$)): MOxCT, 390 (3.71). For the X-ray structure, see Results.

**(k) Fe(DMGBBN)$_2$(PY)$_2$.** The carbonyl complex above was heated in 20 mL of pyridine at 50 °C for 30 min. Hexane was added to induce precipitation. The red solid was filtered out, washed with hexane, and dried in vacuo. Yield: 0.4 g, 72%. Anal. Calcd for $FeC_{34}H_{50}N_6B_2O_4$: C, 59.68; H, 7.37; N, 12.28. Found: C, 59.46; H, 7.18; N, 12.25. $^1H$ NMR ($\delta$, $CDCl_3$): 2.23 (dmg), 8.80, 7.76, 7.28 (PY), 1−2 (BBN). IR ($cm^{-1}$): $\nu_{BH}$ = 2905, 2867, 2829. Vis ($\lambda_{max}$, nm (log $\epsilon$, $M^{-1}$ $cm^{-1}$)): MOxCT, 516 (3.76).

**(l) Fe(DMGBBN)$_2$(BuNH$_2$)$_2$.** Butylamine (0.1 mL) was added to 1 mL of a solution of Fe(BBN)(PY)(CO) (0.01 M) in $CH_2Cl_2$. Long needle crystals formed on standing in room lighting overnight. These were filtered out, dried in air, and then used directly for the X-ray structural determination. Vis ($\lambda_{max}$, nm): MOxCT, 548. For the X-ray structure, see Results.

**(m) In Situ.** Many additional derivatives may be obtained in situ by addition of an excess of ligand L to a dichloromethane solution of $FeN_4(CH_3CN)_2$ or $FeN_4(PY)_2$ and as solids by precipitation with hexane or ether. L = $NH_3$, pip, MeIm, $RNH_2$, $PR_3$, 2,3-dichloro-5,6-dicyano-1,4-benzoquinone (DDQ), 4-nitrophthalonitrile (NPT), (2,4,7-trinitrofluorenyl)malononitrile (TNFMN), etc. For L = $NH_3$, an approximately 1 M solution of $NH_3$ in $CH_2Cl_2$ was used (prepared by shaking concentrated aqueous $NH_3$ with $CH_2Cl_2$). These complexes were characterized by their distinctive visible or NMR spectra which parallel those of Fe(DMGH)$_2$ or Fe(DMGBF$_2$)$_2$ derivatives described previously.[1a,c] Full spectrophotometric titrations and relevant equilibrium constants have been determined in many cases.[5c]

**Spectrophotometric Titrations.** Equilibrium constants for ligand binding were determined spectrophotometrically in $CH_2Cl_2$ from full visible spectra showing large absorbance changes and clean isosbestic points. Typical conditions were [Fe] = $10^{-4}$ M in 1 cm Pyrex cuvettes thermostated at 25 °C. Data covered the full saturation range. For equilibria involving CO, the CO pressure was maintained at 1 atm (total pressure) above the solution. A solubility of CO under these conditions of 0.008 M was assumed on the basis of the Bunsen coefficient for $CHCl_3$. In toluene the reported solubility for CO of 0.007 M was used.

**Kinetic Studies.** Flash photolysis studies were carried out in CO-saturated dichloromethane at 25 °C in 10 cm Pyrex cells as described previously.[6a] Typical conditions: [$FeN_4$] = 0.005−0.01 mM, absorbance changes 0.1−0.5 at $\lambda_{max}$.

Slower reactions involving complexes of MeIm and $BuNH_2$ (the BBN·$BuNH_2$ required flash photolysis) were also followed on a conventional spectrophotometer. Typically, 25 $\mu$L of a 10 mM solution of a bis(amine) complex in $CH_2Cl_2$ was injected into a thermostated cuvette containing 3 mL of CO-saturated solvent ($CH_2Cl_2$ or toluene) with [L] = $10^{-4}$−0.1 M. The reaction was monitored by the decay of the MOxCT band of the bis(amine) complex, and absorbance changes were analyzed by standard methods.

**Electrochemistry.** Electrochemical measurements were carried out on $CH_2Cl_2$ solutions ([$FeN_4$] = 1 mM) with 0.1 M TBAP as the supporting electrolyte. The traditional three-electrode system was used. A platinum disk (0.5 mm diameter) was used as the working electrode, while a large-area platinum wire was used as an auxiliary electrode. A potassium chloride saturated SCE was used as the reference electrode. Cyclic voltammetric and difference square-wave voltammetric data were collected with a Model CYSY-1 computer-controlled electroanalysis system (Cypress Systems Inc.). Half-wave potentials were determined either from cyclic voltammetry at 200 mV/s scan rates or from difference square-wave voltammetry.

**Crystallography.** X-ray-quality crystals were grown by slow diffusion of hexane into $CH_2Cl_2$ solutions of the complexes for the three systems **1** = $BPh_2$, **2** = $BF_2$, and **3** = BBN. The short forms **1-CO** for Fe(DMGBPh$_2$)$_2$(PY)(CO) and **1-BuNH$_2$** for the bis(butylamine) complex are used below. The sparingly soluble **3-BuNH$_2$** complex crystallized directly via the slow reaction of **3-CO** with excess butylamine in $CH_2Cl_2$. Crystals were mounted on glass fibers using epoxy.

Single-crystal X-ray data were collected at room temperature on a Siemens R3m/v diffractometer using graphite-monochromatized Mo K$\alpha$ radiation ($\lambda$ = 0.710 73 Å). Cell parameters were determined from 25 to 40 reflections. Three standard reflections were measured after every 97 reflections. Intensity data were collected using $\theta/2\theta$ scans from 3.5 to 50° in $2\theta$ with variable speeds from 3.00 to 30.00°/min in $\omega$. Absorption corrections based on $\phi$ scans were applied. Linear absorption coefficients, scattering factors, and anomalous dispersion corrections were taken from the usual source.[11a] Structures were solved by direct or Patterson methods followed by Fourier syntheses. Final refinement was done by full-matrix least squares procedures using anisotropic thermal parameters except as noted below. The H atoms were placed in idealized positions and refined isotropically with a riding model. All calculations used the SHELXTL PLUS (PC) package.[11b] Full crystallographic details are given in the supporting information.

**1-CO.** The Fe was located on a special position in *Pbcn* with 2-fold rotational symmetry. The rotation axis runs through the CO and pyridine ligands. A $CH_2Cl_2$ solvent lies on this axis above the CO with its chlorines flanking the pyridine ligand of a neighboring molecule in the lattice.

**2-CO.** The structure was refined in the chiral space group $P2_12_12_1$ and found to consist of one enantiomer whose chirality arises from the twist of the pyridine ligand. The correct configuration was determined on the basis of the Rogers parameter[11c] which refined to $\eta$ = 1.01(7) in the final least squares cycle. A $CH_2Cl_2$ solvent was located and refined with ordered chlorines but with disorder of the $CH_2$ group.

**3-CO.** Direct methods produced a pseudosolution in the correct space group $P2_1/n$ which would not refine below $R$ = 0.35. A direct methods solution in the space group $P1$ correctly located the four molecules of the unit cell. A translation of the origin produced symmetry conforming to that of $P2_1/n$. With this location of the asymmetric unit, the structure refined without further complication in $P2_1/n$ to a final $R$ of 0.067.

**1-Bu.** The Fe atom lies on a center of symmetry with only half of the molecule making up the asymmetric unit.

**2-Bu.** This structure was refined in the hexagonal space group $R\bar{3}$. The iron atom lies on a center of symmetry with half of the molecule making up the asymmetric unit.

(11) (a) *International Tables for X-ray Crystallography*; Kynoch Press: Birmingham, U.K., 1974; Vol. 4. (b) Sheldrick, G. M. *SHELXTL PC*, Version 4.1; Siemens Analytical X-Ray Instruments Inc.: Madison, WI, 1990. (c) Rogers, D. *Acta Crystallogr.* **1981**, *A37*, 734.

**3-Bu.** The structure was refined in the noncentrosymmetric space group *Cc*. Attempts to refine in $C_{2c}$ produced unacceptable distortions in the Fe−N bond and BBN groups and several NPD's. The chirality parameter[11c] refined to $\eta = 0.05(14)$.

## Results

**Synthesis and Ligation.** Boron-derivatized complexes[5] are obtained in high yield by reaction of the substitution-inert[6a] Fe(DMGH)$_2$(py)(CO) with common boron reagents as shown in eqs 1−3 (DMGH = dimethylglyoximate, PY = pyridine,

$$Fe(DMGH)_2(PY)(CO) + 2BH_3Me_2S \rightarrow Fe(DMGBH_2)_2(PY)(CO) + 2H_2 + 2Me_2S \quad (1)$$

$$Fe(DMGH)_2(PY)(CO) + 2BBN\text{-}H \rightarrow Fe(DMGBBN)_2(PY)(CO) + 2H_2 \quad (2)$$

$$Fe(DMGH)_2(PY)(CO) + (Ph_2B)_2O \rightarrow Fe(DMGBPh_2)_2(PY)(CO) + H_2O \quad (3)$$

BBN−H = 9-borabicyclo[3.3.1]nonane). An alternative route to a Fe(DMGBPh$_2$)$_2$(MeIM)$_2$ complex has been previously reported.[13]

Direct treatment of the labile Fe(DMGH)$_2$(PY)$_2$ complex with boron reagents typically produces the tris clathrochelate species Fe(DMG)$_3$(BR)$_2$ described by Rose,[14] Gryzbowski,[15] and Reedijk.[13b] The clathrochelate complexes absorb in the visible region at 440 nm and are substitution inert. The less reactive reagents, dimesitylborane and dicamphanylborane did not react with Fe(DMGH)$_2$(PY)(CO) under mild conditions, and lengthy reaction times or vigorous heating invariably produced clathrochelate species or other uncharacterized products. Successful bis-borylation is favored with reactive boron reagents, and the clathrochelate side reaction and other complications are best avoided when two strong B−R bonds are present. Thus arylboron reagents are preferred to alkylboranes.

Acetonitrile complexes can be obtained in situ from the pyridine derivatives at high dilution ($10^{-5}$ M) in acetonitrile solution and may be titrated with pyridine, giving stepwise binding constants $K_1$ and $K_2$.

$$FeN_4(CH_3CN)_2 + PY \rightleftharpoons FeN_4(CH_3CN)(PY) + CH_3CN \quad K_1 \quad (4)$$

$$FeN_4(CH_3CN)(PY) + PY \rightleftharpoons FeN_4(PY)_2 + CH_3CN \quad K_2 \quad (5)$$

The Fe(DMGBPh$_2$)$_2$(CH$_3$CN)$_2$ complex is insoluble in CH$_3$CN and precipitates from solution dilute enough to drive eq 4 to the left. For the BH$_2$ and BBN systems, this fortuitous route was not available. In addition, labile BH$_2$ and BBN derivatives were found to be significantly more air sensitive than BF$_2$ or BPh$_2$ complexes, consistent with oxidative cleavage of the B−H and B−C bonds leading to uncharacterized products bearing a resemblance to tris clathrochelate species.

Conversion of the Fe(DMGBR$_2$)$_2$(CH$_3$CN)$_2$ or Fe(DMGBR$_2$)$_2$(PY)$_2$ complexes to a variety of axial-ligated derivatives is achieved with complete retention of the boron substituents through ligand substitution reactions exhaustively characterized previously in Fe(DMGH)$_2$ and Fe(DMGBF$_2$)$_2$ systems.[6]

The inert Fe(DMGBH$_2$)$_2$(PY)(CO) complex was examined for possible reactivities of the B−H bond. No facile reactivity was found consistent with observations of Gryzbowski[15b] on the tris clathrochelate Fe(DMG)$_3$(BH)$_2$. Forcing conditions led to decomposition.

**Spectra.**[12] The borylated complexes are distinguished from DMGH analogues by a splitting of the MPyCT bands in the FeN$_4$(PY)$_2$ derivative, $\nu_{CO}$ above 2000 cm$^{-1}$ in the carbonyl complexes, and dmg methyl resonances shifted significantly downfield of the DMGH analogue. There are only slight shifts in the MOxCT bands of the different borylated derivatives, but there are significant shifts of MAxCT bands. The spectral features parallel those fully elucidated in DMGH[9a] and DMGBF$_2$[6a] systems.

The splitting in the MPyCT band of FeN$_4$(PY)$_2$ complexes is quite diagnostic for borylation. In the planar DMGH system, a single broad band is found.[9a] The splitting is believed to be a consequence of the reduced axial symmetry which constrains the orientation of the bound pyridine ligands.

The shifts in the dmg methyl resonance and $\nu_{CO}$ are consistent with electronegativity considerations. The $^1$H NMR resonances of the BH$_2$ and BBN complexes occur at the highest field, while those for complexes with the more electron-withdrawing BF$_2$ and BPh$_2$ substituents lie 0.1−0.2 ppm to lower field. Values of $\nu_{CO}$ for the carbonyl complexes are some 40−70 cm$^{-1}$ higher than those for the DMGH system (1985 cm$^{-1}$ for Fe(DMGH)$_2$(PY)(CO)[9d]). The order for $\nu_{CO}$ (cm$^{-1}$) [2049, BF$_2$ > 2048, BPh$_2$ > 2022, BH$_2$ > 2012, BBN] is consistent with inductive/$\pi$-back-bonding considerations,[16] but additional factors associated with the electric field effects of the axial B−R dipoles positioned in close contact with the CO in a $C_{2v}$ conformation could also be involved.[17]

**Electrochemistry.** Cyclic voltammetry experiments were carried out in CH$_2$Cl$_2$ on the FeN$_4$(PY)$_2$ complexes. The mixed-ligand derivatives were generated in situ and gave distinct reversible oxidation waves for each species with half-wave potentials independent of added ligand concentration. These are assigned to the metal oxidation. For complexes of the electron-deficient nitriles RCN = DDQ, TNFMN, and TCNE, both oxidation and reduction waves are observed. The oxidation wave is assigned to the Fe$^{II/III}$ oxidation giving the Fe$^{III}$ −RCN$^0$ complex. The first reduction wave is assigned to reduction of the coordinated nitrile giving the Fe$^{II}$−RCN$^-$ complex. Reduction potentials for the free ligands were measured independently for comparison. These agree with literature data where known and are given in parentheses along with the other data in Table 2.

**Equilibria.** Equilibrium constants for ligand substitution reactions were measured spectrophotometrically. A typical data set is shown in Figure 2. The results are collected in Figure 3. A detailed thermodynamic analysis of these data was presented previously.[5c]

**Kinetics.** The kinetics for CO binding (eq 6) were studied in dichloromethane solution by the flash photolysis method

$$FeN_4(PY)_2 + CO \rightarrow Fe(N_4)(PY)(CO) + PY \quad (6)$$

(12) Charge transfer bands are abbreviated MOxCT, MPyCT, and MAxCT for metal to oxime, pyridine, or other axial ligand, respectively.

(13) (a) Jansen, J. C.; Verhage, M. *Cryst. Struct. Commun.* **1982**, *11*, 305−307. (b) Verhage, M.; Hoogwater, D. A.; van Bekkum, H.; Reedijk, J. *Recl. Trav. Chim. Pays-Bas* **1982**, *101*, 351−357.

(14) (a) Boston, D. R.; Rose, N. J. *J. Am. Chem. Soc.* **1973**, *95*, 4163−4168. (b) Jackels, S. C.; Rose, N. J. *Inorg. Chem.* **1973**, *12*, 1232−1237.

(15) (a) Gryzbowski, J. J. *Inorg. Chem.* **1985**, *24*, 1125−1126. (b) Robbins, M. K.; Naser, D. W.; Heiland, J. L.; Gryzbowski, J. J. *Inorg. Chem.* **1985**, *24*, 3381−3387.

(16) Timney, J. A. *Inorg. Chem.* **1979**, *18*, 2502−2506.

(17) Oldfield, E.; Guo, K.; Augsberger, J. D.; Dykstra, C. E. *J. Am. Chem. Soc.* **1991**, *113*, 7537−7541.

**Table 1.** Visible Spectral Data[a]: $\lambda_{max}$, nm

| complex | $BPh_2$ | $BF_2$ | $BH_2$ | BBN | H |
|---|---|---|---|---|---|
| $FeN_4(PY)_2$ | 526 | 521 | 523 | 514 | 510 |
| | 378 | 366 | 384 | 381 | 410 bd |
| | 421 | 405 | 429 | 450 | |
| $FeN_4(PY)CO$ | 405 | 404 | 404 | 390 | 392 |
| $FeN_4(BuNH_2)_2$ | 556 | 546 | 536 | 548 | 536 |
| $FeN_4(BuNH_2)CO$ | 403 | 403 | | 400 | |
| $FeN_4(i\text{-}PrNH_2)_2$ | 562 | 544 | | | |
| $FeN_4(NH_3)_2$ | 540 | 531 | | | 532 |
| $FeN_4(PY)(NH_3)$ | 515 | 531 | | | 512 |
| | 380 | 367 | | | 412 |
| $FeN_4(PIP)_2$ | 565 | 557 | 550 | 541 | |
| $FeN_4(MeIM)_2$ | 538 | 535 | 540 | 531 | |
| $FeN_4(MeIM)(PMePh_2)$ | 499 | 498 | | | |
| $FeN_4(CH_3CN)_2$ | 453 | 444 | | | |
| $FeN_4(PY)(TCNE)$ | 430 | 430 | | | |
| | 1100 | 970 | | | |
| $FeN_4(PY)(DDQ)$ | 473 | | | | |
| | 1552 | 1209 | | | |
| $FeN_4(PY)(NPT)$ | 470 | 460 | | | |
| | 625 | 560 sh | | | |
| $FeN_4(PY)(MePZ^+)$ | 480 | 480 | | | |
| | 770 | 695 | | | |
| $FeN_4(PY)(TNFMN)$ | 450 | | | | |
| | 1023 | | | | |

[a] Solvent is $CH_2Cl_2$. MOxCT given first; MAxCT bands given below for Ax = PY, TCNE, NPT, DDQ, $MePz^+$. Extinction coefficients (MOxCT) are typically 7(1) × $10^3$ $M^{-1}$ $cm^{-1}$ for the bis(amine) complexes and 4.5(5) × $10^3$ $M^{-1}$ $cm^{-1}$ for the carbonyls. See Experimental Section for specifics.

**Table 2.** Electrochemical Data: $E_{1/2}$,V vs SCE[a]

| complex | $Fe^{3+/2+}$ | $L/L^-$ [b] |
|---|---|---|
| $Fe(DMGH)_2(PY)_2$ | 0.20[c] | |
| $Fe(DMGBBN)_2(PY)_2$ | 0.46 | |
| $Fe(DMGBH_2)_2(PY)_2$ | 0.61 | |
| $Fe(DMGBF_2)(PY)_2$ | 0.88 | |
| | 0.76[d] | |
| $Fe(DMGBPh_2)(PY)_2$ | 0.62 | |
| $Fe(DMGBPh_2)(PY)(CH_3CN)$ | 0.73 | |
| $Fe(DMGBPh_2)(CH_3CN)_2$ | 0.80 | |
| $Fe(DMGBPh_2)(PY)(NH_3)$ | 0.52 | |
| $Fe(DMGBPh_2)(NH_3)_2$ | 0.36 | |
| $Fe(DMGBPh_2)(PY)(NPT)$ | 0.84 | |
| $Fe(DMGBPh_2)(PY)(DDQ)$ | 1.09 | 0.40 (0.59) |
| $Fe(DMGBPh_2)(PY)(TNFMN)$ | 1.09 | −0.22 (0.03) |
| $Fe(DMGBPh_2)(PY)(TCNE)$ | 1.17 | 0.00 (0.29) |

[a] 0.1 M TBAP in $CH_2Cl_2$; this work unless stated otherwise. [b] Nitrile ligand reduction potential. The free ligand reduction potentials are given in parentheses. [c] Toma, H. E.; Morino, L. A. *Transition Met. Chem.* **1990**, *15*, 66. [d] Data acquired in $CH_3CN$, from ref 6a.

previously used for the $BF_2$ system.[6a] In all cases, photolysis of solutions of the carbonyl complex in the presence of excess pyridine produces $FeN_4(PY)_2$. On the basis of the dissociative mechanism given in eq 7 for the general case, leaving group L, trans ligand T, and entering ligand E, the rate constant for rebinding of CO after the flash under pseudo-first-order conditions in [CO] and [PY] is given by eq 8. When the reverse

$$FeN_4TL \underset{k_{+6}}{\overset{k_{-L}}{\rightleftharpoons}} FeN_4(T) \underset{k_{-E}}{\overset{k_{+E}}{\rightleftharpoons}} FeN_4(T)(E) \qquad (7)$$

$$k_{obs} = (k_{-L}k_{+E}[E] + k_{-E}k_{+L}[L])/(k_{+L}[L] + k_{+E}[E]) \qquad (8)$$

reaction is negligible ($k_{-E}$ term small), linear plots of $1/k_{obs}$ vs [PY]/[CO] are obtained (Figure 4) providing values of the pyridine off-rate constant, $k_{-PY}$, and the competition ratio, $k_{+PY}/k_{+CO}$. Data for the $BF_2$, $BH_2$, BBN, and $BPh_2$ systems are collected in Table 3. New data for the $BF_2$ system were

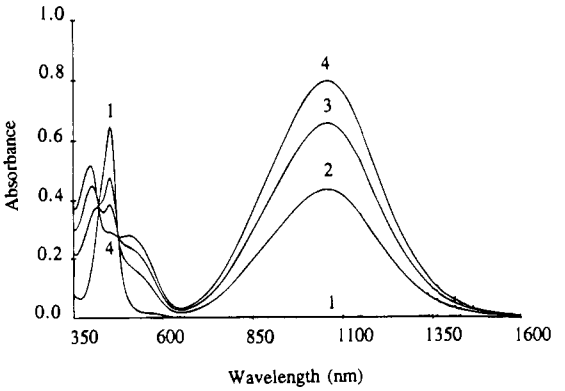


**Figure 2.** Spectrophotometric data for the titration of $Fe(DMGBPh_2)_2(CH_3CN)_2$ with TCNE in 1.0 M $CH_3CN$ in $CH_2Cl_2$. [TCNE] = 0, 0.1, 0.27, and 1.0 mM for curves 1−4.

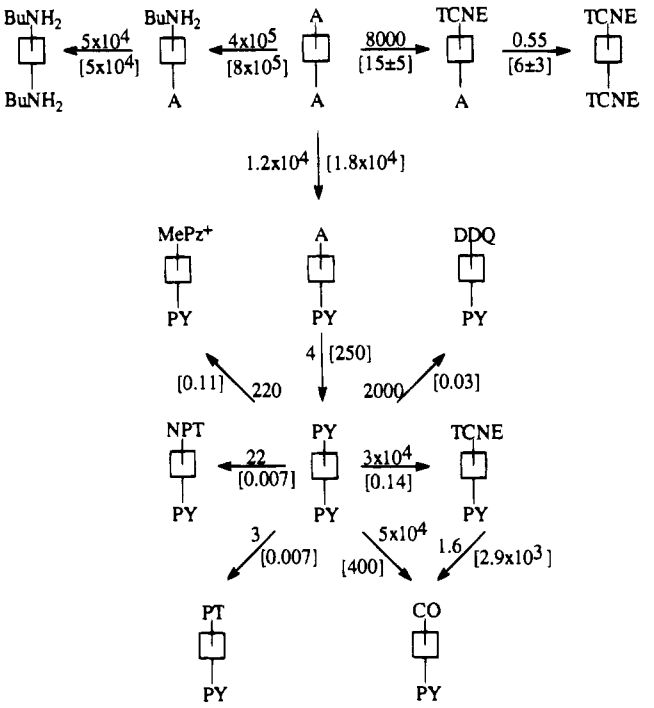


**Figure 3.** Equilibrium constants from spectrophotometric titrations in $CH_2Cl_2$ at 25 °C. Values for the $BPh_2$ complex are given above the arrows, values for the $BF_2$ complex are given below in brackets. A = $CH_3CN$.

obtained in $CH_2Cl_2$, and these are similar to previous results of Thompson obtained in toluene.[6a]

Kinetic studies were also carried out in $CH_2Cl_2$ or toluene solution for the reaction of methylimidazole, piperidine, and butylamine complexes with CO. The methylimidazole and $BuNH_2$ complexes are sufficiently inert to also allow the use of conventional mixing techniques in the rate determinations. Results were the same using flash photolysis and conventional methods.

Kinetic data for the pseudo-first-order approach to equilibrium involving reaction with the bulky methyldiphenylphosphine ligand in reaction 9 were analyzed using eq 8.

$$FeN_4(MeIm)_2 + PMePh_2 \rightarrow FeN_4(MeIm)(PMePh_2) + MeIm \qquad (9)$$

Independent measures of the limiting rates, $k_{-L}$ (MeIm loss) and $k_{-E}$ ($PMePh_2$ loss), were obtained for reaction 9. Absorbance data for the fully equilibrated solutions were analyzed for the overall equilibrium constant, $K$. This value was in good

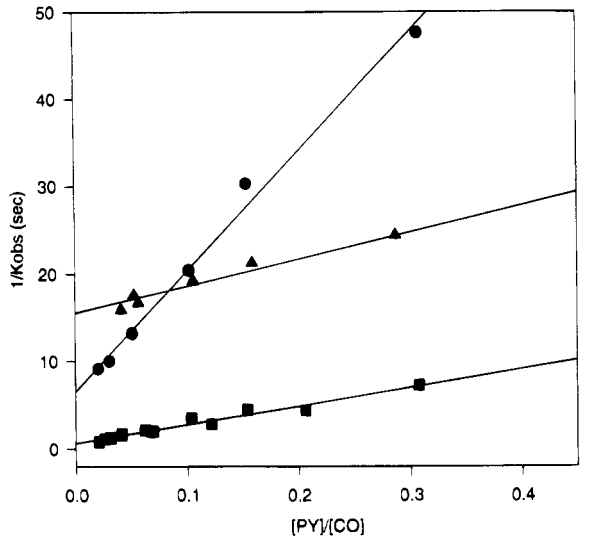


**Figure 4.** Kinetic plots for reaction 6: ●, $BF_2$; ▲, $BPh_2$; ■, $BH_2$. For ▲, $BPh_2$, vertical scale has units of $10^{-2}$ s.

agreement (using eq 12) with parameters derived from the least squares fit of the kinetic data according to eq 8.

A similar approach was taken to the study of the kinetics of the reaction of the Fe(DMGBPh$_2$)(PY)(TCNE) complex shown in eq 10. Data were collected at fixed [CO] and variable

$$FeN_4(PY)(TCNE) + CO \rightarrow FeN_4(PY)(CO) + TCNE \quad (10)$$

[TCNE] and analyzed for both kinetic and equilibrium constants. The equally slow displacements of the TCNE ligand by PY and MeIM were also studied, but both are complicated by secondary processes involving PY-TCNE and MeIM-TCNE charge transfer complexes.

$$FeN_4(PY)(TCNE) + 2PY \rightarrow FeN_4(L_2) + TCNE\text{-}PY \quad (11)$$

Tables of $k_{obs}$ vs ligand concentrations are included as supporting information for all of these reactions, and the derived kinetic parameters are collected in Table 3.

Additional on- and off-rate contants were derived using eq 12, which relates the on- and off-rate constants for the entering

$$K = k_{-L}k_{+E}/k_{-E}k_{+L} \quad (12)$$

group (E) and leaving group (L) to the overall equilibrium constant $K$. Where both kinetic and equilibrium data were obtained, the derived parameters were found to be mutually consistent.

**X-ray Structures.** The results of X-ray structural determinations for the carbonyl and bis(butylamine) complexes in the $BF_2$, $BPh_2$, and BBN systems are shown in Figures 5−10, and crystallographic details are collected in Table 4. A few important strutural parameters are compared in Table 5. Complete listings of positional and thermal parameters, bond lengths, and bond angles are available as supporting information.

For the carbonyls, the $C_{2v}$ conformation, which positions the two axial boron groups on the less hindered face containing the CO ligand, is found in all three cases. The iron and boron atoms lie out of the $N_4$ plane toward the CO ligand with the displacement decreasing in the order $BF_2$ > $BPh_2$ > BBN. The axial-boron-linked groups are significantly pinched inward (Figure 11) in the $BF_2$ system, resulting in close contacts between the fluorines and the carbonyl carbon (2.81 Å). In the $BPh_2$ complex, the axial B−C vectors are approximately perpendicular to the $N_4$ plane, while in the BBN case, a repulsive contact with the apical carbon causes an outward fold of the BBN groups. The apical BBN C−H groups are directed toward the CO ligand and may be responsible for the slight bend of the carbonyl and greater off-rate in this case.

There are also significant differences in the orientation of

**Table 3.** Kinetic Data[a]

Dissociation Constants: $k_{-L}$, $s^{-1}$

| | $BR_2$ | | | |
|---|---|---|---|---|
| $FeN_4TL$[b] | $BF_2$ | $BPh_2$ | $BH_2$ | BBN |
| Fe(PY)(CO) | 0.00002 | 0.00006 | 0.00002 | 0.0002 |
| Fe(PY)$_2$ | 0.15(3) | 6.5(4) | 1.6(2) | 20(1) |
| Fe(BuNH$_2$)$_2$ | 0.013(1) | 0.013(1) | | 21(7) |
| Fe(PIP)$_2$ | 16(2)[c] | 76(8)[c] | | |
| Fe(MeIM)$_2$ | 0.0013(2)[c] | 0.008(1)[c] | 0.014(2)[c] | 0.21(2)[c] |
| Fe(MeIM)(PMePh$_2$) | 0.00056(6)[c] | 0.0008(1)[c] | | |
| Fe(PY)(TCNE) | 4[d] | 0.00062(5) | | |
| Fe(PY)(DDQ) | 10[d] | 0.007(1) | | |
| Fe(PY)(TNFMN) | | 0.20(4) | | |
| Fe(PY)(NPT) | 42[d] | 0.05 (0 °C) | | |
| Fe(PY)(CH$_3$CN) | 37[d] | 27[d] | | |

Discrimination Ratios: $k_{+X}/k_{+Y}$

| | | $BR_2$ | | | |
|---|---|---|---|---|---|
| intermediate | X/Y | $BF_2$ | $BPh_2$ | $BH_2$ | BBN |
| Fe(PY) | PY/CO | 21(3) | 2.0(3) | 33(4) | 28(3) |
| | TCNE/CO | | 5(1) | | |
| | TCNE/PY | | 3(1)[e] | | |
| | DDQ/PY | | 2[e] | | |
| | TNFMN/PY | | 1.3[e] | | |
| Fe(BuNH$_2$) | BuNH$_2$/CO | 56(7) | 7(1) | | 59(7) |
| Fe(MeIM) | MeIm/CO | | 3(1)[c] | | |
| | MeIm/PMePh$_2$ | 2(1)[c] | 5(2)[c] | | |
| Fe(PIP) | PIP/CO | 22(3)[c] | 3(1)[c] | | |

[a] In $CH_2Cl_2$ at 25 °C unless otherwise indicated. [b] Leaving group is listed last. [c] Toluene solution. [d] Calculated from equilibrium data[6c] by assuming $k_{+RCN}/k_{+PY}$ = 1 per nitrile group. [e] Calculated from off-rates and equilibrium constants.

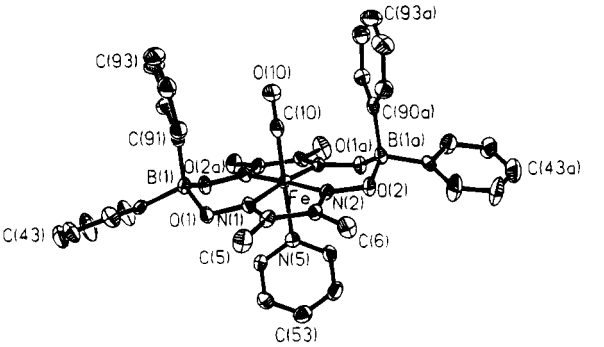


**Figure 5.** Structure of **1-CO** (Fe(DMGBPh$_2$)$_2$(PY)(CO)) with 30% probability thermal ellipsoids.

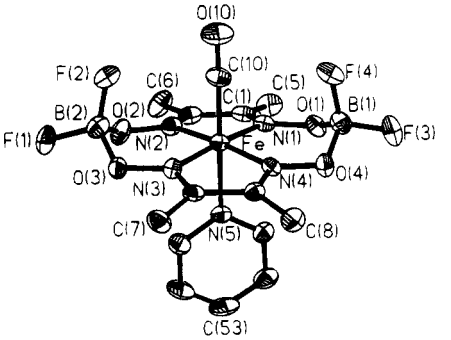


**Figure 6.** Structure of **2-CO** (Fe(DMGBF$_2$)$_2$(PY)(CO)) with 30% probability thermal ellipsoids.

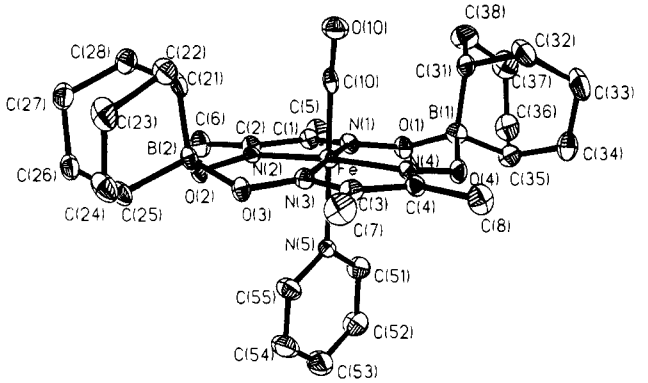


**Figure 7.** Structure of **3-CO** ($Fe(DMGBBN)_2(PY)(CO)$) with 30% probability thermal ellipsoids.

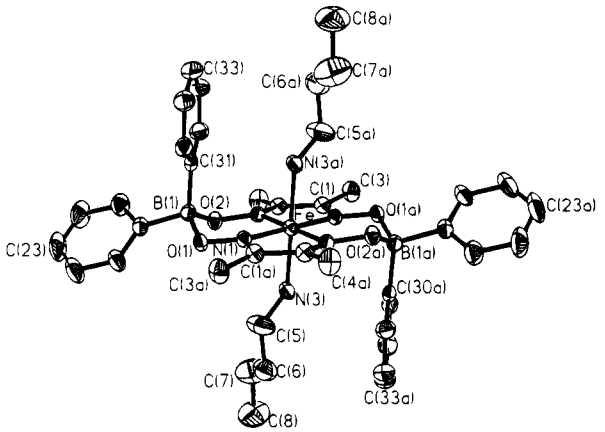


**Figure 8.** Structure of **1-Bu** ($Fe(DMGBPh_2)_2(BuNH_2)_2$) with 30% probability thermal ellipsoids.

the pyridine ligand bound on the open face of the macrocycle. The pyridine plane makes an angle with the B1−B2 vector of 2.6, 13, and 21.6° for $BF_2$, $BPh_2$, and BBN, respectively. This twist correlates qualitatively with the relative pinching ($BF_2$ > $BPh_2$ > BBN) of the axial boron groups on the opposite face.

**$BuNH_2$ Complexes.** All three butylamine derivatives adopt the $C_{2h}$ conformation. The closest heavy atom contacts between the superstructure and the amine nitrogen occur for C(90) in **1**, F(2) in **2**, and C(25) in **3**. Repulsion is the greatest for the BBN case involving the C−H−N contact. The amine N−H groups are directed away from the BBN superstructure in this case. The contacts are the shortest for the $BF_2$ case, where an N−H−F hydrogen bond[18] is indicated on the basis of an N−F distance of 2.87 Å. The directions of the N−H bonds toward the phenyl rings in **1-Bu** are consistent with weak N−H $\pi$ interactions.

In addition to the intramolecular H-bond indicated in **2-Bu**, there also is an intermolecular H-bond linking the other N−H group and an equatorial fluorine of an adjacent molecule in the lattice. The $N-F_{eq}$ distance is 3.0 Å. The orientation of the $BuNH_2$ ligand in the crystal serves to optimize both types of H-bonds.

Interactions between the $BuNH_2$ ligand and the superstructure do not cause significant bending of the axial N−Fe−N axis. Instead, this axis is increasingly tilted (+ is tilted away from the axial $BR_2$) with respect to the $N_4$ plane at angles of −1.8° ($BF_2$), +3.2° ($BPh_2$), and +7.5° (BBN). This tilt is a geometrically simple response to the nonbonded contacts and axial asymmetry in the $C_{2h}$ conformer.

(18) Hamilton, W. A.; Ibers, J. A. *Hydrogen Bonding in Solids*; Benjamin: Reading, MA, 1974.

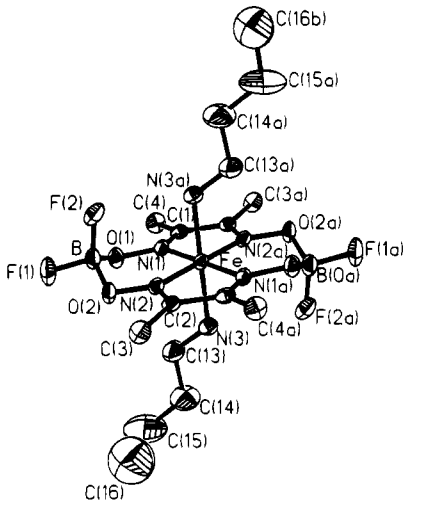


**Figure 9.** Structure of **2-Bu** ($Fe(DMGBF_2)_2(BuNH_2)_2$) with 30% probability thermal ellipsoids.

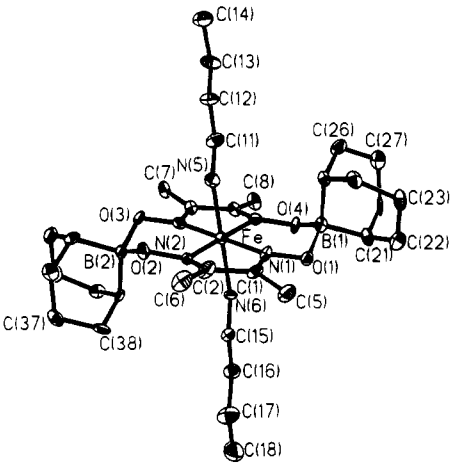


**Figure 10.** Structure of **3-Bu** ($Fe(DMGBBN)_2(BuNH_2)_2$) with 30% probability thermal ellipsoids.

## Discussion

**Electronic Effects and Spectra.** The borylation of (dioximato)iron complexes provides a simple means of varying the electronic character of the iron. Electronic effects are most evident in the $Fe^{II/III}$ redox potentials of the $FeN_4(PY)_2$ derivatives. The trends in $E°$ are in the direction expected on the basis of the electron-donating/withdrawing character of the B−R groups. The BBN group is the most electron donating, $BH_2$ and $BPh_2$ are intermediate, and the $BF_2$ group is the most electron withdrawing. The CO stretching frequencies in the carbonyl complexes are lowest for the BBN case and highest for the $BF_2$ case. As noted previously in the $BF_2$ system,[6a] the $BR_2$ groups have only minor effects on the MOxCT bands in the visible spectrum. It appears that the $BR_2$ groups lower the energy of both the metal and oxime $\pi^*$ orbitals associated with the MOxCT transition, resulting in a cancellation of effects. The charge transfer to the axial ligands (MAxCT in Table 1) provides a clearer indication of the greater ease of metal oxidation in the order $BF_2$ < $BPh_2$ = $BH_2$ < BBN.

**Electrochemistry.** The $Fe^{III/II}$ potentials provide a measure of the effect of the various $BR_2$ groups on the electron density at the iron. The effects seen in the $FeN_4(PY)_2$ complexes, $BF_2$ < $BPh_2$ = $BH_2$ < BBN, are similar to those reported by Gryzbowski for tris clathrochelate species.[15a] In a series of $Fe(DMG)_3(BR)_2$ complexes the iron potentials span approximately

**Table 4.** Crystallographic Data Summary[a]

| | 1-CO | 2-CO | 3-CO | 1-Bu | 2-Bu | 3-Bu |
|---|---|---|---|---|---|---|
| fw | 806.1 | 573.7 | 999.9 | 760.4 | 528.0 | 671.3 |
| space group | *Pbcn* | $P2_12_12_1$ | $P2_1/n$ | $P2_1/n$ | $R\bar{3}$ | *Cc* |
| *a*, Å | 14.943(3) | 12.436(3) | 11.611(2) | 13.928(3) | 27.874(4) | 9.029(4) |
| *b*, Å | 15.890(3) | 13.246(2) | 19.512(3) | 9.845(2) | 27.874(4) | 19.308(9) |
| *c*, Å | 16.211(3) | 14.158(3) | 14.907(2) | 15.288(3) | 8.443(2) | 20.56(1) |
| α, deg | 90 | 90 | 90 | 90 | 90 | 90 |
| *β*, deg | 90 | 90 | 108.53 | 105.86(3) | 90 | 92.790(1) |
| *γ*, deg | 90 | 90 | 90 | 90 | 120 | 90 |
| *V*, Å$^3$ | 3849.2(13) | 2332.2(11) | 3202(10) | 2016.5(7) | 5681(2) | 3590(3) |
| *Z* | 4 | 4 | 4 | 2 | 9 | 4 |
| $\mu$, mm$^{-1}$ | 0.581 | 0.945 | 0.517 | 0.421 | 0.659 | 0.463 |
| $\varrho$, g cm$^{-3}$ | 1.391 | 1.634 | 1.313 | 1.252 | 1.389 | 1.242 |
| index ranges | | | | | | |
| *h* | 0 to 17 | −1 to 13 | −1 to 13 | −1 to 16 | −1 to 31 | −1 to 10 |
| *k* | 0 to 18 | −1 to 18 | −1 to 23 | −1 to 11 | −33 to 1 | −1 to 22 |
| *l* | 0 to 19 | −1 to 19 | −17 to 17 | −18 to 17 | −1 to 10 | −24 to 24 |
| total no. of reflns | 3405 | 4339 | 6932 | 4492 | 2871 | 4081 |
| no. of reflns with $I > 4\sigma(I)$ | 1438 ($2.5\sigma(I)$) | 2699 | 2718 | 2312 | 1256 | 2412 |
| no. of params | 249 | 314 | 388 | 242 | 152 | 405 |
| largest diff, e Å$^{-3}$ | | | | | | |
| peak | 0.28 | 0.45 | 0.50 | 0.58 | 0.34 | 0.63 |
| hole | −0.35 | −0.50 | −0.64 | −0.30 | −0.44 | −0.39 |
| GOF | 0.93 | 1.23 | 1.23 | 1.48 | 1.27 | 1.12 |
| $R$ ($I > 4\sigma(I)$) | 0.056 | 0.051 | 0.065 | 0.059 | 0.058 | 0.060 |
| $R_w$ | 0.055 | 0.058 | 0.066 | 0.072 | 0.063 | 0.063 |

[a] Scan type $\theta/2\theta$; scan range $3.5° < 2\theta < 50°$.

**Table 5.** Comparative Structural Data for $BPh_2$, $BF_2$, and BBN Complexes (Å, deg)

| | 1-CO | 2-CO | 3-CO | 1-Bu | 2-Bu | 3-Bu |
|---|---|---|---|---|---|---|
| $FeN_4$ | 1.886(5) | 1.892(4) | 1.891(4) | 1.884(4) | 1.877(6) | 1.895(9) |
| Fe−$N_{ax}$ | 2.067(8) | 2.055(5) | 2.068(5) | 2.053(4) | 2.047(4) | 2.036(10) |
| Fe−CO | 1.786(12) | 1.772(6) | 1.771(7) | | | |
| C−O | 1.145(14) | 1.147(8) | 1.144(9) | | | |
| Fe−C−O/Fe−N−$C_\alpha$ | 180.0(1) | 179.0(6) | 175.0(6) | 126.4(4) | 124.4(5) | 123.3(8) |
| $\theta$(amine)[a] | 2.5 | 13.2 | 21.3 | 68 | 24.8 | 78 |
| $\Delta$Fe[b] | 0.079 | 0.082 | 0.058 | 0.0 | 0.0 | 0.0 |
| $\Delta$B[c] | 0.446 | 0.57 | 0.36 | 0.36 | 0.476 | 0.27 |
| B−B[d] | 6.370 | 6.193 | 6.501 | 6.406 | 6.210 | 6.445 |
| axial contacts | C(90) | F(2) | C(35) | C(90) | F(2) | C(25) |
| C10/N5 | 3.14 | 2.81 | 3.45 | 3.18 | 2.87 | 3.54 |
| O10 | 3.30 | 3.00 | 3.59 | | | |

[a] Angle between vertical plane through borons and Fe and the PY or Fe−N−$C_\alpha$ plane. [b] Displacement of Fe from $N_4$ plane. [c] Displacement of B from $N_4$ plane. [d] Distance between borons.

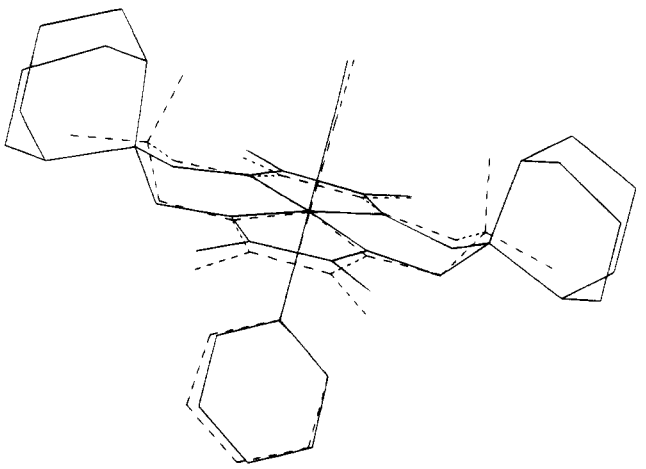

**Figure 11.** Superposiiton of the structures of **2-CO** (dotted lines) and **3-CO** showing the relative pinching of the axial boron groups.

200 mV from R = F to R = $CH_3$. This is about half the range we find for the $Fe(DMGBR_2)_2(PY)_2$ complexes covering a comparable range of substituents. The bis complexes have twice the number of R groups as the tris species, leading to a doubling of the effect.

Much larger variations in $Fe^{III/II}$ potential are found as a function of the nature of the axial ligands. Extensive data pertaining to ligand effects have been previously reported for the $Fe(DMGBF_2)_2$ system.[6a] Since the axial ligand effects vary in a manner qualitatively predictable on the basis of ligand parameters, $E_L$, described by Lever,[19] only a limited set of datafor the $Fe(DMGBPh_2)_2$ system was obtained here. The trends clearly parallel those found earlier for the $BF_2$ system.

Shifts of $E_{1/2}$ (V) are easily estimated for any $(DMGBR_2)_2$ or L combinations by using the electrochemical parameters of Lever.[19] For example, $E_L$ parameters predict a shift of −0.18 per ligand replacement of PY by $NH_3$.[20] The observed stepwise shifts are −0.10 and −0.16. Corresponding data for the $CH_3CN$ complexes: predicted shift, +0.09 per PY replaced by $CH_3CN$; observed, +0.11 and +0.07.

In the $Fe(DMGBPh_2)_2$ case, $\pi$-attractive interactions between the axial phenyls and electron-deficient nitriles result in significant enhancement in the nitrile binding constants for L = TCNE, DDQ, NPT, and TMFMN and slow (on the E-chem time scale) nitrile ligand exchange rates. This allows us to measure the effects of these good $\pi$-acceptor nitriles on the

(19) Lever, A. B. P. *Inorg. Chem.* **1990**, *29*, 1271−1285.
(20) The $E_L$ parameters are based on data acquired in $CH_3CN$ and may not apply exactly to the $CH_2Cl_2$ data reported here.

$Fe^{II/III}$ potentials as well as the corresponding effect of the metal on the nitrile ligand reduction potential.

As the nitrile becomes a better acceptor, $CH_3CN$ < NPT < DDQ, TNFMN < TCNE, the metal oxidation shifts to higher potentials. The ligand reduction is more favorable when the ligand is coordinated to the iron. Delocalization serves to stabilize the system in both cases, making it more difficult to remove an electron while making it easier to add one. The site of electron gain or loss is unambiguous as the alternatives (nitrile oxidation, reduction to $Fe^{I}$) are unreasonable.

There is an important distinction to be made between these complexes and most other TCNE metal derivatives.[21] Since TCNE, like other nitriles, is normally a rather poor ligand, binding of TCNE is often found in metal complexes which are formally oxidized by TCNE producing the $M^{ox}-TCNE^{-}$ derivative. The metal oxidation potential in $Fe(DMGBR_2)_2$ systems is well above the range where formal oxidation of the metal by TCNE is possible. However, the favorable characteristics of the $Fe(DMGBPh_2)_2$ system for the observation of weak ligand binding (low-spin $d^6$, noncoordinating solvent) and the dramatic effects of peripheral phenyl TCNE contacts combine to produce a very inert $Fe^{II}-TCNE^{0}$ complex.

To summarize the various redox-tuning strategies demonstrated here: $BR_2$ variations span 0.42 V from BBN to $BF_2$, axial ligand variations can span over a volt, and delocalization within axial nitrile ligands can contribute as much as 0.5 V.

**Structure and Conformation.** Conformations were established in the $BPh_2$ system on the basis of the ring current shifted resonances.[5a,c] These results suggested that 1,4 diaxial contacts in the (boroximato)iron chelate rings (between BR groups and axial ligands) were the prime determinant of the favored conformation. In the absence of information to the contrary, one can only assume that similar considerations apply to all borylated dioxime complexes. The structures for the BBN, $BF_2$, and $BPh_2$ complexes reported here support this assumption.

The carbonyl complexes all adopt the $C_{2v}$ structure, and the bis-$BuNH_2$ complexes all adopt the $C_{2h}$ conformation. The $C_{2v}$ conformer is also found for a series of $BPh_2$ derivatives, $Fe(DMGBPh_2)_2(PY)X$, X = $PMePh_2$ (axial phenyl on PY face), $NH_3$, and TCNE, reported separately.[5d] The centrosymmetric $C_{2h}$ conformation is found in the X-ray structures of all three bis-$BuNH_2$ complexes reported here and also in $Fe(DMGBPh_2)_2(MeIm)_2$,[13b] $Fe(DMGBPh_2)_2(CH_3CN)_2$, and $Fe(DMGBPh_2)_2(CH_3CH_2CH_2CN)_2$.[5d]

However, the $C_{2v}$ conformation is unexpectedly found in the crystal structures[5d] of $Fe(DMGBPh_2)_2(PY)_2$ and $Fe(DMGBF_2)_2(4\text{-tBuPY})_2$. This suggests that the $C_{2h}$ and $C_{2v}$ conformations have quite similar energies in the bis(pyridine) derivatives.

The structures of the $BPh_2$, $BF_2$, and BBN complexes do not show any unusual distortions of the basic $FeN_4$ macrocycle as a result of appending the different $BR_2$ groups in either conformation. This is especially important when one seeks to use differences in ligational energetics between the systems as measures solely of electronic effects and axial nonbonded interactions. Buckling, doming, ruffling, and other distortions are introduced in the porphyrin ligand in some of the superstructured hemes.[2f]

The tilting of the axial bond axis in the $C_{2h}$ structures and the opening or closing of the superstructure gates in the $C_{2v}$ conformer represent very simple reaction coordinates on the conformational energy surface of these complexes. Because of the conformational simplicity in these systems, relationships among structure, conformation, and the dynamics of axial ligation are more tractable.

(21) Kaim, W.; Moscherosch, M. *Coord. Chem. Rev.* **1994**, *129*, 157.

**Kinetics.** In considering the connection between conformational and ligational dynamics, it is necessary to apply the Curtin–Hammett principle[22] to each step in the mechanism (eq 7). The overall ligand substitution process consists of a dissociative step (ligation barrier ≫ conformational barrier) and an addition step (ligation barrier ≈ conformational barrier). Shifts of BR groups from equatorial to axial positions are not an energetically significant component of the reaction coordinate for dissociation. The barriers associated with ligand addition however are quite small[9c] ($k_+ = 10^8\ M^{-1}\ s^{-1}$) and therefore factors associated with conformational motion can and do[2a,7a] play a significant role in the on-rates.

**Off-Rate Effects.** The off-rate constants and trends in binding equilibria reflect the general ligand binding strength order $CH_3CN$ < PIP < PY < $BuNH_2$ < MeIm < $PMePh_2$ < CO typically found in iron dioxime systems. The effects of borylation are consistent with a combination of electronic and steric effects. Good $\sigma$ donors are labilized as the donor ability of $BR_2$ increases in the order $BF_2$ < $BPh_2$ < $BH_2$ < BBN. However electronic effects on lability are not very large, as seen in the near coincidence of many rates for the $Fe(DMGH)_2$ and $Fe(DMGBF_2)_2$ systems.[5a]

The larger off-rate constants found in the $BPh_2$ and BBN systems clearly have a significant component associated with steric effects. The trends seen in Table 3 reflect many of the structural evidences of nonbonded interactions cited above. Off-rates for the various nitriles reflect attractive interactions beween the nitriles and axial phenyls. These are shown to arise from Coulombic forces between the positive regions of the electron-deficient nitriles and the negative $\pi$-face of the phenyl groups.[5c]

**Bond Length vs Bond Strength.** The off-rate constants are a good measure of the metal–ligand bond strength in these systems.[23] It is noteworthy that the differences in the metal–ligand bonding indicated in the rate data are not reflected in the metal ligand bond lengths. The CO off rate constants show a small but significant difference while the Fe–C bond lengths do not. The $Fe-N_{py}$ distances trans to CO are longer than those found in the $FeN_4(PY)_2$ complexes, yet pyridine is at least 6 orders of magnitude more inert trans to CO. The $BuNH_2$ ligand is 3 orders of magnitude more labile in **3-Bu** than in **1-Bu** or **2-Bu**, yet the Fe–N bond length is the shortest in **3-Bu**.

Comparisons with structural and ligational data for hemes further document the point. Heme carbonyl bond lengths[24a] are comparable to those reported here, yet the CO off-rates are 1000 times faster. In general, many low-spin heme axial bond lengths[24b] are comparable to those found in these $FeN_4$ systems yet the labilities differ dramatically.[9b]

These apparent contradictions cannot be ignored or assigned to some mysterious transition state effect. The notion that bond lengths are measures of bond strength and kinetic data are "something else" is a widespread fallacy. **The metal–ligand bond energy includes the sum of all effects throughout the molecule which accompany coordinate bond dissociation.** The off-rate constant is the best available measure of this energy.

(22) Curtin, D. Y. *Rec. Chem. Prog.* **1954**, *15*, 111. Eliel, E. *J. Chem. Educ.* **1960**, *37*, 126.

(23) The case here is made in terms of activation free energy, which mirrors effects in bond enthalpies in these systems. The use of dissociative activation energies as measures of bond enthalpy is not new: Halpern, J.; Ng, F. T.; Rempel, G. L. *J. Am. Chem. Soc.* **1979**, *101*, 7124–7126.

(24) (a) Peng, S. M.; Ibers, J. A. *J. Am. Chem. Soc.* **1976**, *98*, 8032–8036. (b) Scheidt, W. R.; Reed, C. A. *Chem. Rev.* **1981**, *81*, 543–555.

**Bond length measures a local phenomenon between the metal and the donor atom.**[25]

This is no more dramatically shown than in the nitrile complexes, especially $Fe(DMGBPh_2)_2(PY)(TCNE)$. Only minimal effects on the iron−TCNE bond energy are associated with the low-energy metal to TCNE charge transfer. The low-energy MAxCT is found in both $BF_2$ and $BPh_2$ systems, yet TCNE becomes unusually inert **only** in the $BPh_2$ complex. The additional binding energy in the $BPh_2$ complex is to be found in the Coulombic attraction between the bound TCNE and the peripheral phenyl groups. This Coulombic contribution to the bond energy is largely invisible to X-ray crystallography.[5d]

Significant delocalization of electron density involving the metal and the TCNE ligand is evident from the redox data presented above and in bond lengths within the TCNE ligand in the $Fe(DMGBPh_2)_2(PY)(TCNE)$ complex.[5d] These are not likely to be much different in the $BF_2$ analogue, and they do not contribute significantly to the coordinate bond energy. Electron density is redistributed in a metal complex on forming and on breaking a metal ligand bond. Some local bonds are strengthened at the expense of others which are weakened. Most of the energy associated with this redistribution may be self-canceling. When enhancements in the Fe−N bond are made at the expense of the weakening of other bonds or vice versa, the Fe−N bond length is not representative of its binding energy. This explains in a very simple way why bond lengths, spectroscopic data, and other measures of localized bonding often do not agree with global measures of coordinate bond energy.

**On-Rate Effects.** On-rate constants in unhindered hemes are typically $10^7$ $M^{-1}$ $s^{-1}$ for CO[9c] and around $(2-4) \times 10^8$ $M^{-1}$ $s^{-1}$ for most other ligands.[26] A ratio of 10−20 is typically found for $k_{+L}/k_{+CO}$ in heme and $FeN_4$ systems. The on-rate constant ratios $k_{+X}/k_{+Y}$ are a measure of the ability of the pentacoordinate intermediate to discriminate between entering ligands.

It may be reasonably assumed that the pentacoordinate intermediate adopts a $C_{2v}$ geometry as found in the carbonyl complexes but with significantly greater displacement of the iron out of the $N_4$ plane. The recently obtained structure of a pentacoordinate ($\mu$-oxo)diiron complex[6e] provides a good indication of the structural consequences of pentacoordination in the $Fe(DMGBPh_2)_2$ system. In this complex the iron lies 0.3 Å out of the $N_4$ plane toward the oxo ligand, while on the distal side the two axial phenyl groups collapse to partially fill the trans void. A view of this cavity in the ligated and unligated forms is shown in Figure 12. Binding within the cavity requires an opening of these "gates". We believe the differences in the on-rate constants for the $BPh_2$ complexes in Table 3 reflect the energetics associated with the opening of these gates. It should be noted that only in the $BPh_2$ system does the superstructure extend much more than 3 Å above the iron. Thus the $BPh_2$ system is the only system of the three studied here where repulsions with the entering ligand are encountered well in advance of any significant bonding interaction with the iron.

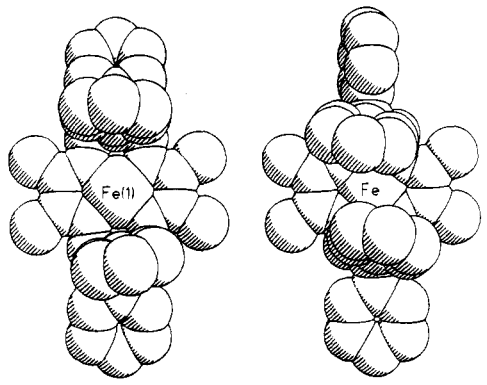


**Figure 12.** View of the binding cavity in the $BPh_2$ system in the ligated (left) and unligated (right) geometries based upon $\mu$-oxo structures.[6e] A $BuNH_2$ ligand bound to Fe(1) has been removed to reveal the cavity size.

Discrimination ratios for amine vs CO addition to $Fe(DMGBPh_2)_2$ intermediates are consistently about 10 times smaller than those for the other systems. This effect is found for L = PY, MeIm, PIP, and $BuNH_2$. The discrimination ratios for the $BuNH_2$ complexes are greater than those for the other ligands. This seems to reflect the greater nucleophilicity of the more basic amines rather than any hydrogen-bonding effect which could be considered for the $BF_2$ case. The similar pattern observed in the discrimination ratios for PY and $BuNH_2$ also rules out the possibility that some unusual trans effect on CO or PY addition is involved in the $BPh_2$ system. Of all the ligands studied, CO is unique[7a] in being able to enter the cyclophane-like cavity with a minimum of opening of the "gates". The other ligands all require a significant opening of the cavity. An opening of the cavity in the transition state is to be distinguished from a 90° flip of an axial phenyl to the equatorial position, as found in some of the products. In the addition of CO, PY, or $PMePh_2$ to the $Fe(DMGBPh_2)_2(PY)$ intermediate, 0, 1, and 2 axial phenyls are flipped to the opposite face in the product. Because the barrier for conformational flipping is small, the axial groups are easily pushed away by the larger ligands, producing the products in their stable conformations.

The on-rate effects observed here may be compared with those found in the more rigid hindered cyclophane hemes.[2a] Increasingly bulky ligands produce increasingly larger effects in Traylor's cyclophane hemes. In contrast, the on-rate effects found for $k_{+L}/k_{+CO}$ in the $Fe(DMGBPh_2)_2$ system disappear for $k_{+MeIm}/k_{+PMePh_2}$. We believe these different patterns of discrimination in the on-rate reflect the fundamentally different nature of the conformational free energy surface for these two systems. In the heme cyclophane system, the conformational strain associated with swinging the anthracene cap increases with increasing deformation. Thus larger ligands encounter greater entering barriers. In flipping the boroximate ring, the axial phenyls are rotated through 90°. The flip barrier profile may reach a maximum very early (e.g., for a 10° rotation). Ligands requiring a greater opening of the cavity thus experience no greater repulsion than those requiring much smaller distortion in the transition state.

This on-rate effect is also apparent in the photochromic properties of the carbonyl complexes.[27] The photogenerated pentacoordinate $BF_2$ intermediate is efficiently trapped in CO-saturated solvent at $[BuNH_2]$ or [PY] = 0.0001 M, producing a pink color even in room light. The corresponding $BPh_2$ species requires a 10-fold higher concentration of the amine to

(25) The notion of a "localized bond energy" considered to reside between the two bonded atoms is pedagogically unsound. Only in the vacuously satisfied case of diatomics or for average bond energies based on heats of atomization of molecules is this concept valid. In polyatomic molecules, there can be no experimental measure of individual bond energies other than that derived from the energy required to break the bonds one at a time.

(26) Dixon, D. W.; Kirmaier, C.; Holten, D. *J. Am. Chem. Soc.* **1985**, *107*, 808−813. (b) Lavellette, D.; Tetreau, C.; Momenteau, M. *J. Am. Chem. Soc.* **1979**, *101*, 5395−5401.

(27) Chen, X.; Stynes, D. V. *Inorg. Chem.* **1987**, *26*, 3145−3151.

achieve the same result. We have carefully examined the efficiency of trapping of the photogenerated pentacoordinate intermediate as a function of [PY]/[CO] via flash photolysis. The ratios $k_{+PY}/k_{+CO}$ derived from trapping studies (microsecond time scale) in the $BF_2$ and $BPh_2$ systems are identical to those obtained from the slower time scale kinetic studies (0.1 s) of reaction 6. Much faster time scale experiments are required to reveal events associated with the opening or closing of the gates in the pentacoordinate intermediate.[2d]

The on-rate results given above confirm and extend previous ideas[2a] concerning conformational effects on the dynamics of ligation of a guest to a site within a superstructured host. The extent to which on-rates are lowered by groups which block access to the binding site depends upon relationships betweeen the conformational free energy surface of the host and the steric demands of the guest. These relationships are perhaps most fully elucidated in the binding of ligands to the vacant coordination site of the pentacoordinate iron in $Fe(DMGBPh_2)_2$, cyclophane hemes,[2a] and myoglobin.[7a]

**Acknowledgment.** Financial support from York University and NSERC of Canada is gratefully acknowledged.

**Supporting Information Available:** A table of kinetic data and complete listings of atomic coordinates, thermal parameters, bond lengths and angles, and hydrogen atom positions for **1-CO**, **2-CO**, **3-CO**, **1-Bu**, **2-Bu**, and **3-Bu** (33 pages). This material is available in many libraries on microfiche, immediately follows this article in the microfilm version of the journal, and can be ordered from ACS; see any current masthead page for ordering information.

IC950196H